Supporting Information

# Key Factors Dominating Photoelectrochemical Performance of g-$C_3N_4$ Polymer films

Qiushi Ruan, Mustafa K Bayazit, Vankayala Kiran, Jijia Xie, Yiou Wang, Junwang Tang*

**Abstract: we investigated the relationship among crystallinity, deep trap states and PEC performance of the g-$C_3N_4$ photoelectrodes. Long-lived charge carriers are present in samples with worse crystallinity due to deeper trap states, which inversely correlates with photoelectrochemical performance. The charge diffusion length in g-$C_3N_4$ film has been determined to be ca. 1000 nm.**

## Experimental Methods

Sample synthesis

The bulk-g-$C_3N_4$ film, compact-g-$C_3N_4$ film and porous-g-$C_3N_4$ film have been fabricated by three different methods.

Bulk-g-$C_3N_4$ film synthesis:

G-$C_3N_4$ powders were synthesized by heat Dicyandiamide (Alfa Aesar, 99%) at 600°C for 4h in air in a Muffle furnace (Carbolite, CWF 1300). 10 mg as-prepared g-$C_3N_4$ powders were mixed with 750 ml DI $H_2O$ and 250 ml 2-propanol (Fisher Chemical, HPLC grade) and 10 µl Nafion perfluorinated resin solution (Sigma-Aldrich). The suspension was sonicated for 1h and drop-casted onto a 2 cm*2 cm FTO substrate on a 250 °C preheated hotplate. The as-synthesized film was calcined at 400 °C for 30 min to remove the organic residues.

Compact-g-$C_3N_4$ film synthesis (modified rapid thermal vapor condensation method):

50 mg Dicyandiamide (Alfa Aesar, 99%) was dissolved with DI water in a Φ35 mm petri dish. After drying at 70 °C for 1h, Dicyandiamide precursor were recrystallized and adhered to the internal surface of the petri dish. A piece of 2 cm × 2 cm FTO glass used as the substrate was placed on a slightly concave crucible lid and covered by the petri dish. The sample was calcined in a 600 °C preheated Muffle furnace (Carbolite, CWF 1300) for 23 min and quenched to the room temperature in air.

Porous-g-$C_3N_4$ film synthesis:

A FTO substrate was firstly pre-treated by a rapid thermal vapor condensation method at 600 °C for 25 min to make it a more suitable place for carbon nitride nucleation and polymerization. After treatment, there is no visible carbon nitride left on the substrate. The treated FTO was then place on a 10 ml

crucible (FTO side downward) filled with 2 g Dicyandiamide (DCDA). A flat crucible lid was placed above FTO. The crucible was calcined at 600 °C for 4 h with a heating rate of 5 °C/min.

Characterizations

XRD patterns were collected by a D8 Bruker Diffractometer. The FWMH of peaks were analysed by the Match software. Raman spectroscopic measurements were performed on a Renishaw InVia Raman Microscope, using a 325nm excitation laser and a wavenumber range from 200 – 2000 $cm^{-1}$. The UV-Vis absorption spectra were collected using a Shimadzu UV-Vis 2550 spectrophotometer fitted with an integrating sphere using $BaSO_4$ as the reference material. FTIR spectroscopy was performed on a Perkin-Elmer 1605 FT-IR spectrometer in the wavenumber range from 400 – 4000 $cm^{-1}$ with a resolution of 0.5 $cm^{-1}$. XPS measurements were done on a Thermoscientific XPS K-alpha surface analysis machine using an Al source. Analysis was performed on the Casa XPS software. SEM images were taken by a JEOL JSM-7401F Scanning Electron Microscope.

Photoelectrochemical measurements

The photoelectrochemical properties were investigated in a conventional three-electrode cell using an electrochemical analyser (IVIUM Technologies). The as-prepared film, a Pt net and an Ag/AgCl electrode were used as the working, counter and reference electrodes, respectively. The photocurrent of samples was measured in 0.1 M $Na_2SO_4$ aqueous solution under 150 W Xenon lamp (Newport). Samples were illuminated from the SE side (FTO substrate/semiconductor interface). Electrochemical impedance spectra (EIS) were measured from -0.3 V to 0.5 V vs. AgCl/Ag. A sinusoidal ac perturbation of 5 mV was applied to the electrode over the frequency range 0.1 Hz−10 kHz.

In the open-circuit voltage decay (OCVD) measurement, electrodes were placed in dark condition until the voltage became stable. 150 W Xenon lamp (Newport) was illuminated to the EE side of the electrode. After the stable photovoltage was observed, light source was turned off to obtain the photovoltage decay. The electrolyte–electrode (EE) side of each sample was exposed to intense irradiation to generate a photovoltage.

In the small perturbation photovoltage transient (TPV) measurement, a strong continuous light source was irradiated to the sample to excite electron-hole pairs continuously. After the equilibrium between charges generation and charge consumption (recombination and reaction) was achieved, a single pulse generated by UV light-emitting diodes (LEDs, 365nm) was irradiated to the EE side of the electrode. The duration is 1ms. The photovoltage rise and decay corresponding to the pulse light was recorded and used for electron diffusion length calculation. The time constant for photovoltage rise and decay $\tau_{rise}$ and $\tau_n$ was calculated using the initial phase of photovoltage rise and decay with equation (a).

$$\tau = -\frac{K_B T}{q}\left(\frac{dV_{oc}}{dt}\right)^{-1}$$ Equation (a)

Where $k_B$ is the Boltzmann constant, T is the temperature (in Kelvin), and q is the unsigned charge of an electron.

The electron diffusion coefficient was used to calculated using the equation (b)[1]:

$$D_n = \frac{d^2}{\pi^2}\left(1 + \frac{3}{1 + \left(\frac{3}{\sqrt{2}} - 1\right)\frac{C_{C3N4}}{C_{sub}}}\right)\left(\frac{1}{\tau_{rise}} - \frac{1}{\tau_n}\right)$$ Equation (b)

Where d is the thickness of the film; $C_{c3n4}$ and $C_{sub}$ is the capacitance of carbon nitride film and FTO substrate (derived from Figure S9); $\tau_{rise}$ is the time constant of photovoltage rise; $\tau_n$ is the time constant of photovoltage decay.

The diffusion length L was calculated using the equation (c).

$$L = (D_n \tau_n)^{1/2}$$ Equation (c)

**Results**

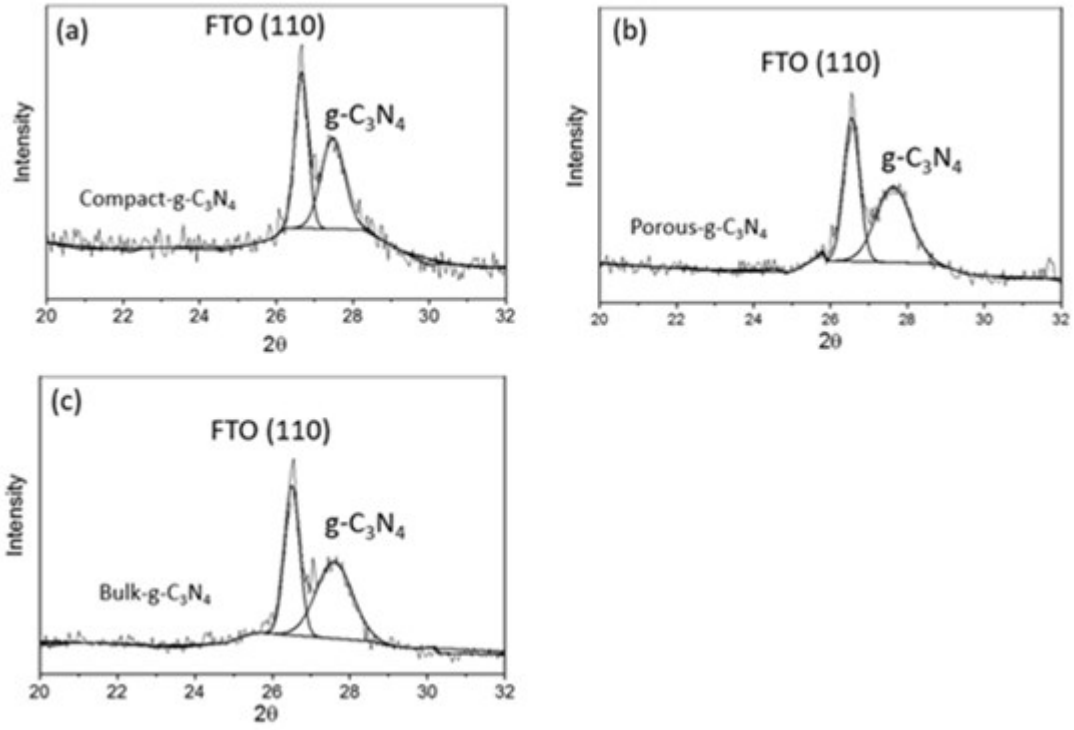


Figure S1 XRD patterns showing peaks of FTO (110) plane and g-$C_3N_4$ stacking layer structure of (a) bulk-g-$C_3N_4$, (b) compact-g-$C_3N_4$ (c) porous-g-$C_3N_4$

And another peak was observed at 26.7° and was assigned to the (110) plane of $SnO_2$ from the FTO

substrate. The full width at half maximum (FWHM) of the XRD $SnO_2$ (110) peak and the g-$C_3N_4$ stacking layer (27.5°) peak were carefully analyzed for each of the three samples to illustrate the crystallinity of the graphite-like layer structure.

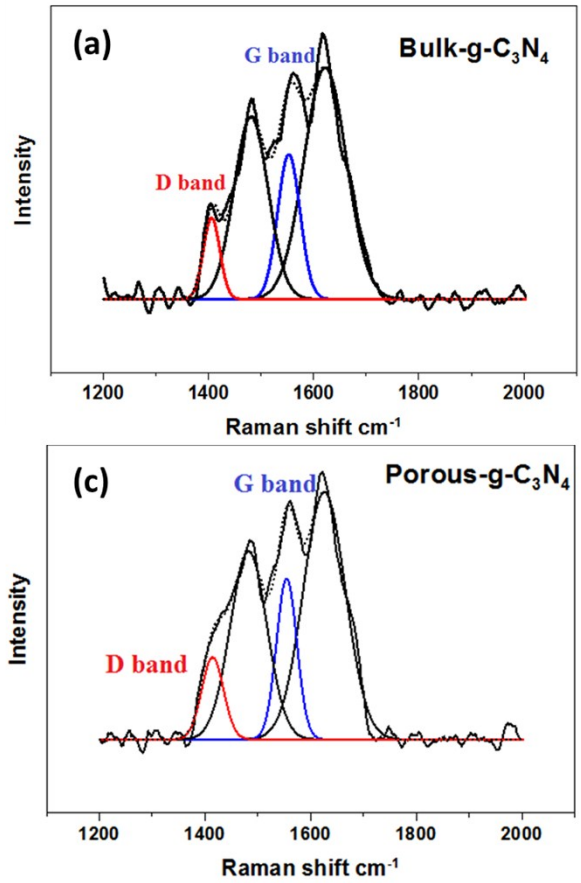


(d)

| sample | $I_D/I_G$ |
|---|---|
| Bulk-g-$C_3N_4$ | 0.41 |
| Compact-g-$C_3N_4$ | 0.13 |
| Porous-g-$C_3N_4$ | 0.55 |

Figure S2 Raman spectra showing different degrees of structural distortion of (a) bulk-g-$C_3N_4$, (b) compact-g-$C_3N_4$ (c) porous-g-$C_3N_4$; (d) the value of $I_D/I_G$ of all three g-$C_3N_4$ samples. The Raman spectra were recorded with exciting laser at 325 nm.

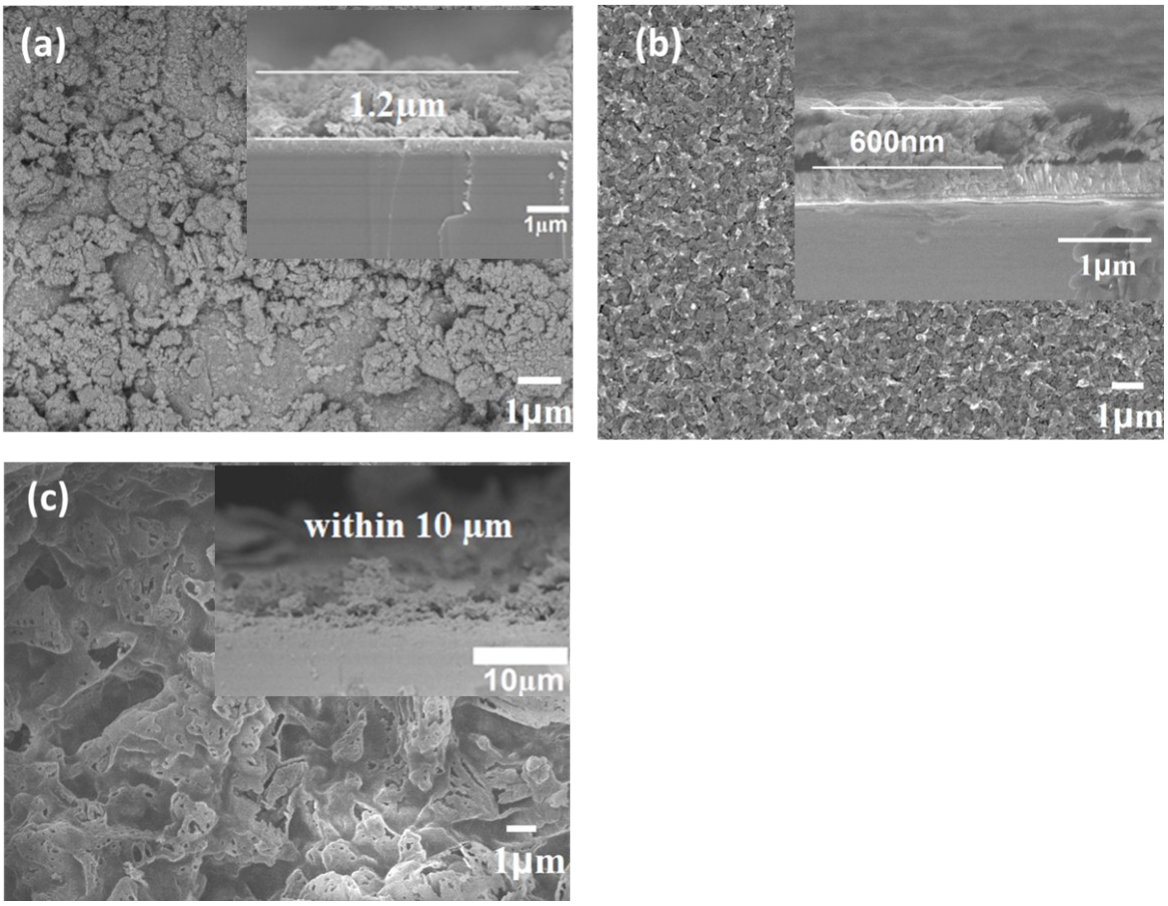


Figure S3 SEM images of (a) bulk-g-$C_3N_4$ film top view and side view (inset), (b) compact-g-$C_3N_4$ film top view and side view (inset), (c) porous-g-$C_3N_4$ film top view and side view (inset).

SEM images show significantly different morphologies for bulk-g-$C_3N_4$ film, compact-g-$C_3N_4$ film and porous-g-$C_3N_4$ film as represented in Figure S3a, b and c, respectively. Apparently, bulk-g-$C_3N_4$ film was composed of aggregation of small particles with uneven distribution (Figure S3a). Even the film is not very uniform, the thickness can be roughly observed to be ca. 1.2 μm. The compact-g-$C_3N_4$ film exhibits a uniform and dense morphology (Figure S3b). The thickness of compact-g-$C_3N_4$ film was measured to be ~600 nm from its cross section image (Figure S3b inset). The uniform and thin film is expected to be beneficial for efficient charge migration and collection across the film in a PEC reaction. The porous-g-$C_3N_4$ film shows a rough surface with hollow structure (Figure S3c), whose thickness varies within 10 μm. The porous structure is likely to have large surface area, a plenty of defects and surface states which have a complicated influence on charge trap, transfer and recombination process.[2]

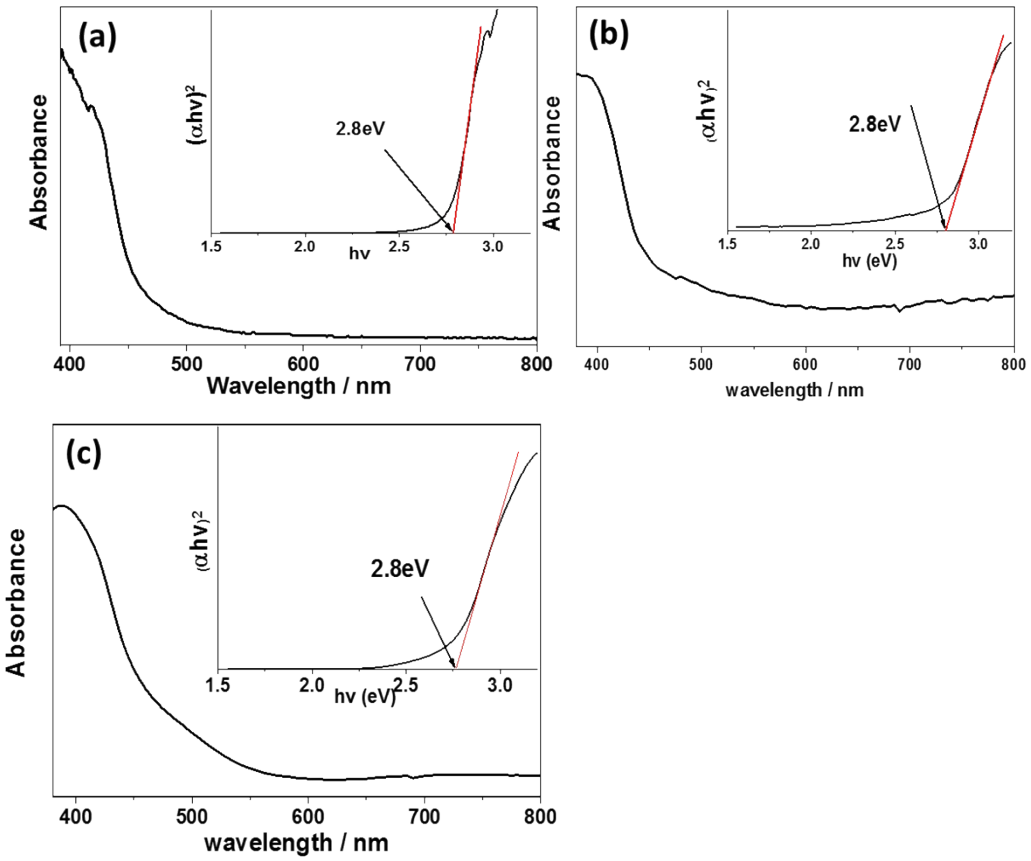


Figure S4 UV-Vis spectra of (a) bulk-g-$C_3N_4$ (b) compact-g-$C_3N_4$ film and (c) porous-g-$C_3N_4$ film

UV-Vis spectra of all samples show very similar absorption edges around 440nm (Figure S4) and band gaps of 2.8eV, derived from the Tauc plot (inset in Figure S4), which is in good consistence with pristine carbon nitride.[3]

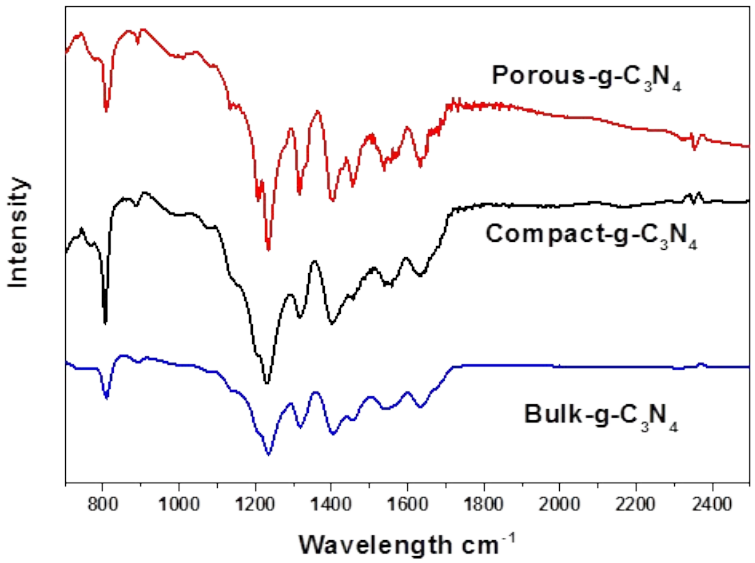


Figure S5 FTIR spectrum of bulk-g-$C_3N_4$ film, compact-g-$C_3N_4$ film and porous-g-$C_3N_4$ film

The FT-IR spectra of all samples are represented in Figure S5. The intense band at 806 $cm^{-1}$ is attributed to the out-of-plane bending vibrations of tri-s-triazine; The bands at 1226 $cm^{-1}$ and 1311 $cm^{-1}$ could be assigned to stretching vibration of C–N(–C)–C or C–NH–C units; The intense bands at 1406 $cm^{-1}$, 1456 $cm^{-1}$, 1558 $cm^{-1}$ and 1633 $cm^{-1}$ represent typical stretching vibration modes of heptazine-derived repeating units.[4]

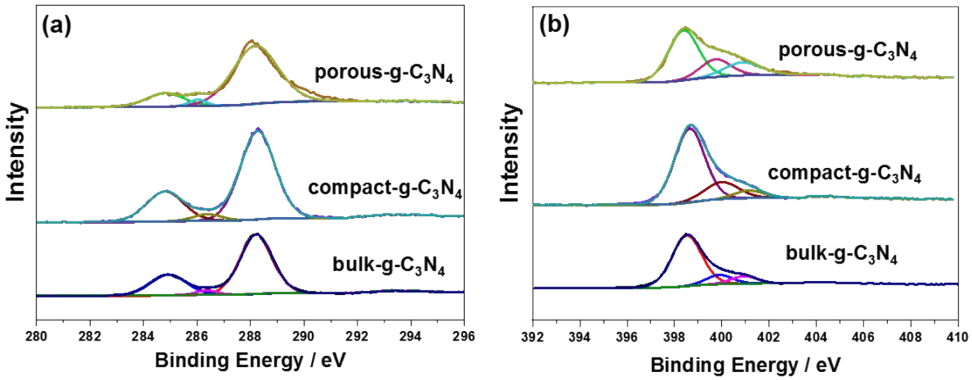


Figure S6 (a) XPS C1s spectra and (b) XPS N1s spectra of bulk-g-$C_3N_4$ film, compact-g-$C_3N_4$ film and porous-g-$C_3N_4$ film

As shown in Figure S6a, the C1s XPS spectra show a peak at 288.1 eV corresponds to the binding energy of C-N-C bonds. The faint peak at 286.2 eV corresponds to C-O bonds and the peak centered at 284.8 eV is adventitious carbon.

Table S1. Percentage of different bonds within the N1s spectra (in Figure S6b) of porous-g-$C_3N_4$ film, bulk-g-$C_3N_4$ film and compact-g-$C_3N_4$ film

| Bond | Binding Energy (eV) | Atomic % of bond (sample) | | |
|---|---|---|---|---|
| | | Porous-g-$C_3N_4$ | Bulk-g-$C_3N_4$ | Compact-g-$C_3N_4$ |
| C-N-C | 398.7 | 60.0% | 71.8% | 72.8% |
| N-$[C]_3$ | 399.9 | 21.2% | 14.6% | 19.2% |
| C-$NH_x$ | 401.1 | 18.8% | 13.6% | 8% |

Table S2. C to N ratio in porous-g-$C_3N_4$ film, bulk-g-$C_3N_4$ film and compact-g-$C_3N_4$ film derived from XPS spectra

| Sample | $C_XN_Y$ |
|---|---|
| Porous-g-$C_3N_4$ | $C_3N_{3.79}$ |
| Bulk-g-$C_3N_4$ | $C_3N_{3.76}$ |
| Compact-g-$C_3N_4$ | $C_3N_{4.12}$ |

Furthermore, the C to N ratios in compact-g-C3N4, bulk-g-C3N4, and porous-g-C3N4 were calculated from the XPS spectra to be $C_3N_{4.12}$, $C_3N_{3.76}$ and $C_3N_{3.79}$ (Table S2, ESI†), indicating that the C/N ratio in compact-g-$C_3N_4$ was the closest to the ideal ratio of 3 : 4.

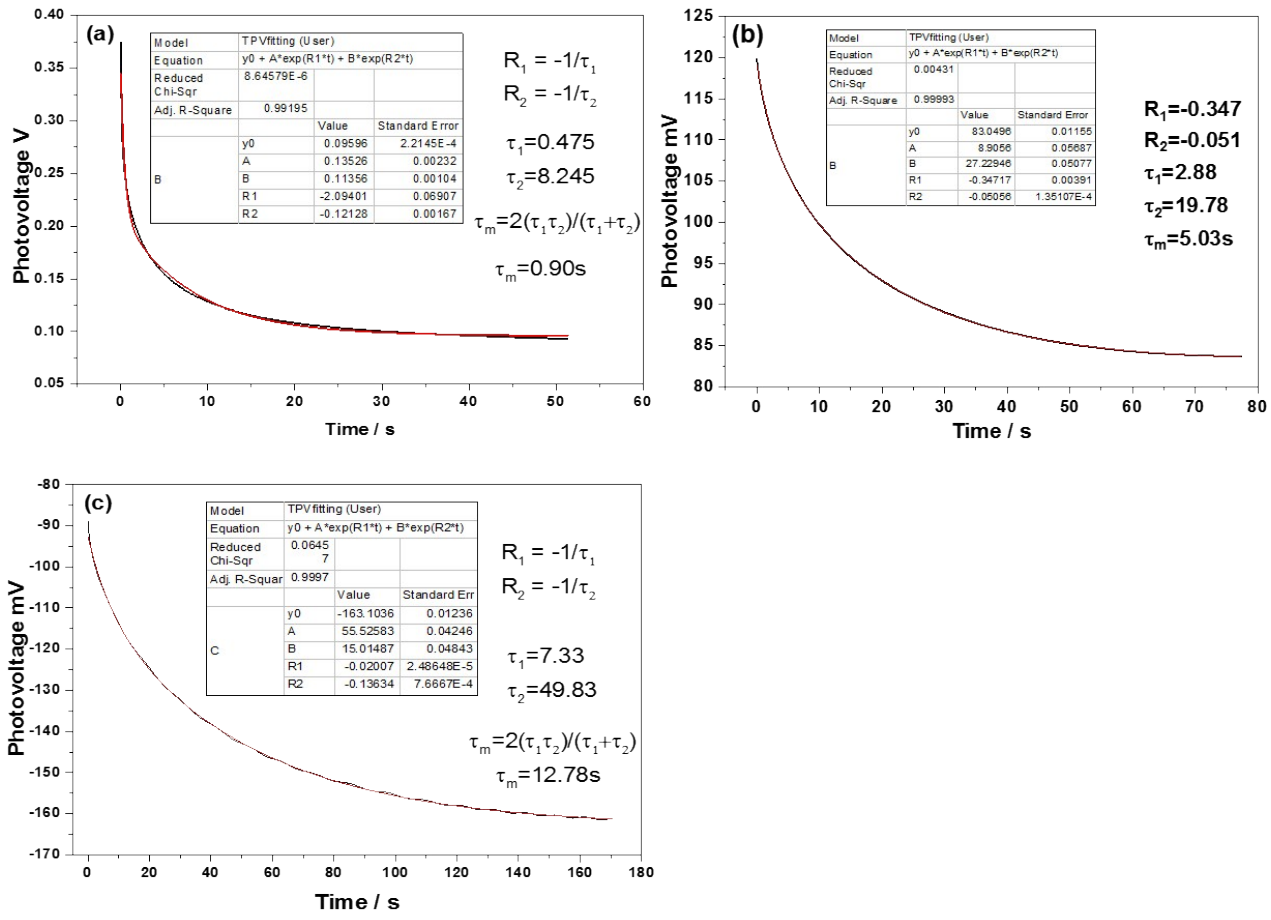


Figure S7 Determination of average electron lifetimes $\tau_m$ by a biexponential fitting in (a) compact-g-$C_3N_4$ film (b) bulk-g-$C_3N_4$ film and (c) poorous-g-$C_3N_4$ film.

In Figure S7, by fitting the decay curve to a biexponential function (equation d and e) as shown below, the average charge lifetime was determined to be 0.9 s, 5.0 s ad 12.8 s for compact-g-$C_3N_4$, bulk-g-$C_3N_4$ and porous-g-$C_3N_4$, respectively.

$$y = A * e^{-\frac{t}{\tau_1}} + B * e^{-\frac{t}{\tau_2}} + C \quad \text{(Equation d)}$$

$$\tau = \frac{2\tau_1\tau_2}{(\tau_1 + \tau_2)} \quad \text{(Equation e)}$$

Where τ is the average lifetime of charges, A, B, C are constant.

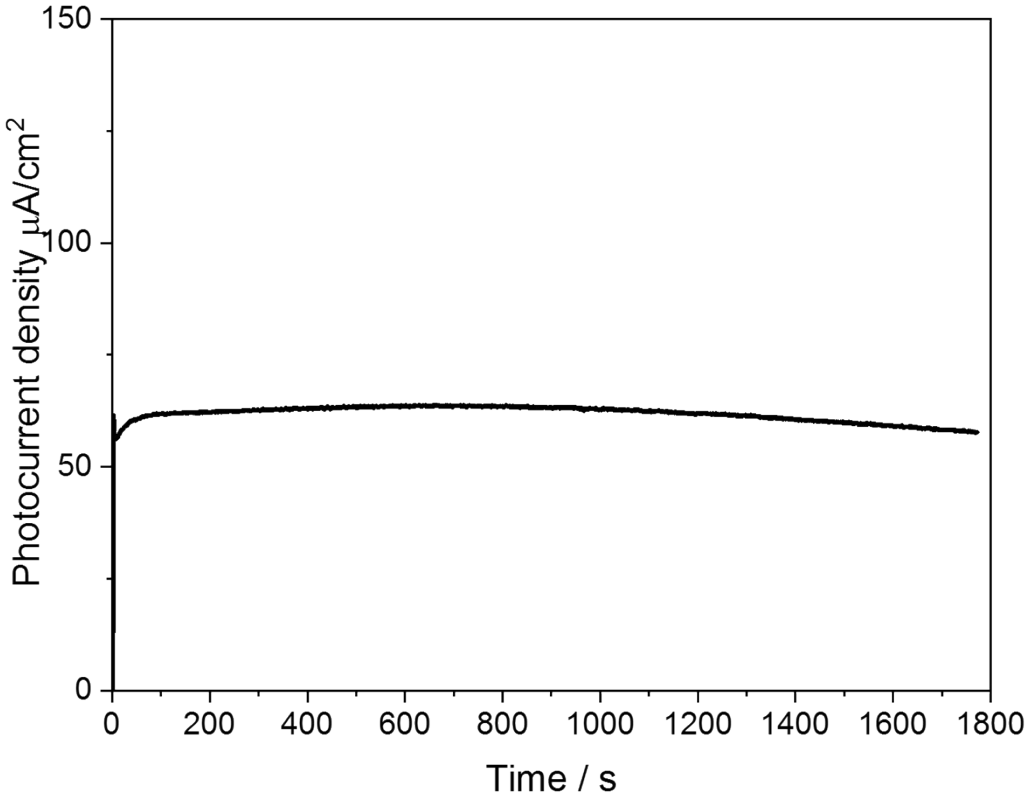


Figure S8 I-T measurement of compact-g-$C_3N_4$ photoelectrode at +0.1V vs Ag/AgCl.

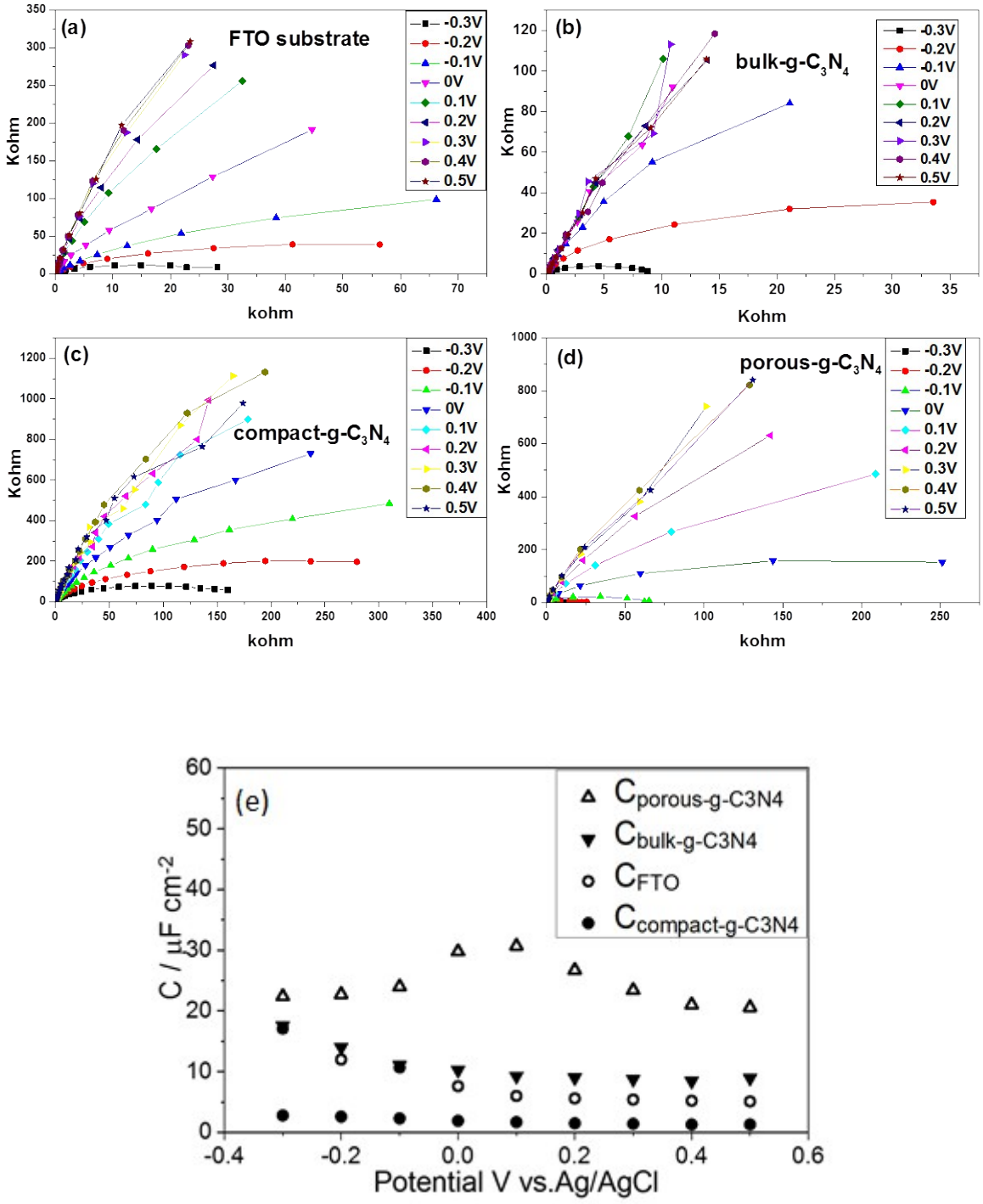


Figure S9 EIS spectra of (a) FTO substrate, (b) bulk-g-$C_3N_4$ film, (c) compact-g-$C_3N_4$ film and (d) porous-g-$C_3N_4$ film; potential range -0.3V to 0.5V vs.Ag/AgCl; frequency 10 KHz to 0.1Hz; amplitude: 0.01V. (e) Capacitance of bulk-g-$C_3N_4$ film, compact-g-$C_3N_4$ film, porous-g-$C_3N_4$ film and FTO substrate.

The capacitances of the bulk-g-$C_3N_4$ film, compact-g-$C_3N_4$ film, porous-g-$C_3N_4$ film and FTO substrate at different potentials are also derived from the impedance plots (Figure S9). The bulk-g-$C_3N_4$ film, compact-g-$C_3N_4$ film, porous-g-$C_3N_4$ film and FTO substrate show the capacitance of 10.8μF $cm^{-2}$, 1.9μF $cm^{-2}$, 24.6μF $cm^{-2}$ and 8.3μF $cm^{-2}$, respectively. Apparently, bulk-g-$C_3N_4$ film and porous-g-$C_3N_4$

film exhibit 6 and 13 times higher capacitance than the compact-g-$C_3N_4$ film due their non-uniform morphology/severe trap states[1]. It is noticed that compact-g-$C_3N_4$ film only has a 1/4 capacitance as that of the FTO substrate. Although, the compact-g-$C_3N_4$ film grow on the top of FTO surface, the high quality carbon nitride film screens the electronic effect of FTO substrate well and results in the lower capacitance.[5]

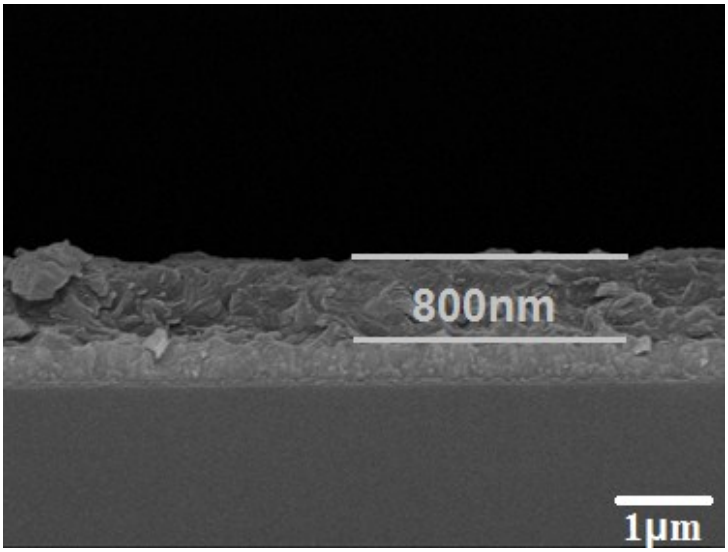


Figure S10 side SEM side view of g-$C_3N_4$ S1 sample

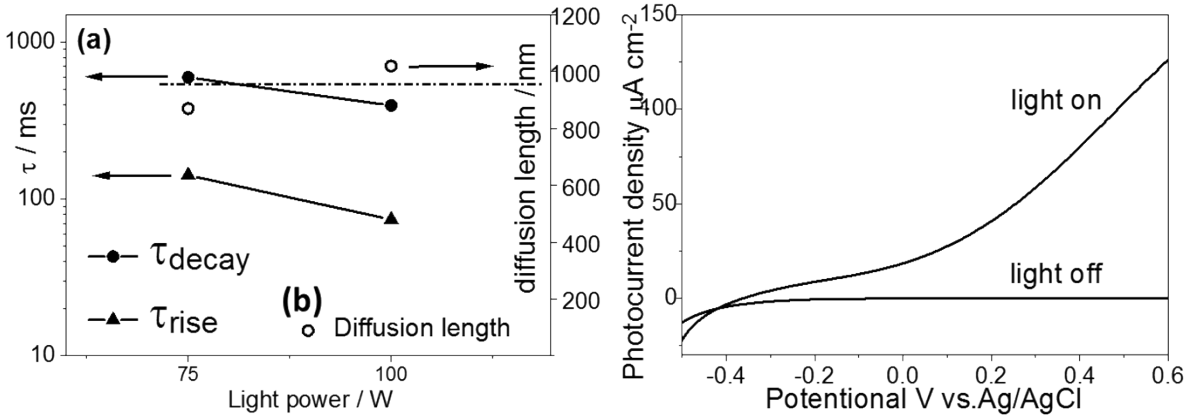


Figure S11 (a) Dependence of photovoltage rise time ($\tau_{rise}$), effective electron lifetime ($\tau_n$) and charge diffusion length of light power of g-$C_3N_4$ S1 sample. (b) photocurrent density vs potential plot of S1 sample using 150W Xenon lamp illuminating from the substrate-electrode (SE) side.

To further confirm the electron diffusion length, TPV measurements were performed on another sample S1 which was also prepared by the rapid thermal vapor condensation method. By adjusting the synthesis time, the thickness of sample S1 was manipulated to 800 nm (in Figure S10). The diffusion length determined form TPV measurements against different pulse intensities were plotted in Figure S11a. The average charge diffusion length was determined to be 950 nm. It suggests that the charge diffusion length does not significantly change with the thickness of the films, at least in the range studied in this work. Thus the average electron diffusion length of the g-$C_3N_4$ film fabricated by the rapid thermal

vapor condensation method is about 1000 nm. Photocurrent response of sample S1 is shown in Figure S11b. The photocurrent density is ca. 130μA $cm^{-2}$ at 0.6 V vs. Ag/AgCl, which is smaller than that observed in the 600nm thick compact-g-$C_3N_4$ film (180μA $cm^{-2}$), while it is still 20 times higher than the bulk g-$C_3N_4$. It is reasonable that a film thickness smaller than its charge diffusion length is beneficial for its PEC performance.

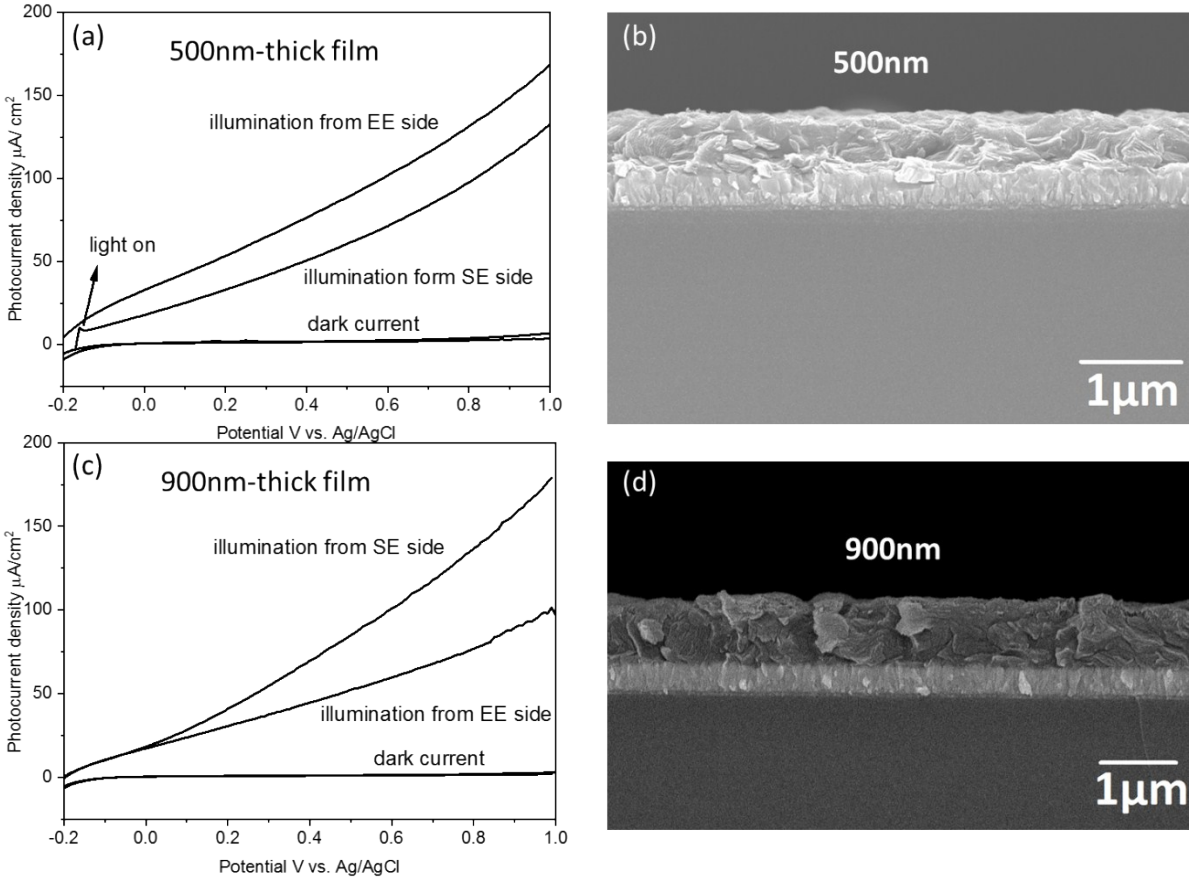


Figure S12. (a) I-V curve of a 500 nm-thick compact-g-$C_3N_4$ film with illumination from EE (electrode/electrolyte) and SE (substrate/electrolyte) side; (b) SEM side view of the 500 nm-thick compact-g-$C_3N_4$ film; (c) I-V curve of a 900 nm-thick compact-g-$C_3N_4$ film with illumination from EE (electrode/electrolyte) and SE (substrate/electrolyte) side; (d) SEM side view of the 900 nm-thick compact-g-$C_3N_4$ film. The film of ca. 500 nm thick is much thinner than our calculated diffusion length (1000nm). The other sample has a thickness of ca. 900 nm which is very close to the calculated diffusion length.

1. W. Leng, P. R. Barnes, M. Juozapavicius, B. C. O'Regan and J. R. Durrant, *The Journal of Physical Chemistry Letters*, 2010, 1, 967-972.
2. A. G. Agrios and P. Pichat, *Journal of Photochemistry and Photobiology A: Chemistry*, 2006, 180, 130-135.
3. Y. Wang, X. Wang and M. Antonietti, *Angewandte Chemie International Edition*, 2012, 51, 68-89.
4. D. J. Martin, K. Qiu, S. A. Shevlin, A. D. Handoko, X. Chen, Z. Guo and J. Tang, *Angewandte Chemie International Edition*, 2014, 53, 9240-9245.
5. A. ter Heijne, D. Liu, M. Sulonen, T. Sleutels and F. Fabregat-Santiago, *Journal of Power Sources*, 2018, 400, 533-538.